Pitkänen et al. Geosci. Lett. (2021) 8:3
https://doi.org/10.1186/s40562-020-00171-7

Geoscience Letters

RESEARCH LETTER

Open Access

Asymmetry in the Earth's magnetotail neutral sheet rotation due to IMF B_y sign?

Timo Pitkänen[1,2,3*], Anita Kullen[4], Lei Cai[4], Jong-Sun Park[1], Heikki Vanhamäki[3], Maria Hamrin[2], Anita T. Aikio[3], G. Siung Chong[2], Alexandre De Spiegeleer[2] and Quanqi Shi[1]

Abstract

Evidence suggests that a non-zero dawn–dusk interplanetary magnetic field (IMF B_y) can cause a rotation of the cross-tail current sheet/neutral sheet around its axis aligned with the Sun–Earth line in Earth's magnetotail. We use Geotail, THEMIS and Cluster data to statistically investigate how the rotation of the neutral sheet depends on the sign and magnitude of IMF B_y. In our dataset, we find that in the tail range of $-30 < \mathrm{XGSM} < -15\,R_E$, the degree of the neutral sheet rotation is clearly smaller, there appears no significant rotation or even, the rotation is clearly to an unexpected direction for negative IMF B_y, compared to positive IMF B_y. Comparison to a model by Tsyganenko et al. (2015, doi:10.5194/angeo-33-1-2015) suggests that this asymmetry in the neutral sheet rotation between positive and negative IMF B_y conditions is too large to be explained only by the currently known factors. The possible cause of the asymmetry remains unclear.

Keywords: Solar wind–magnetosphere interaction, Magnetosphere configuration, Magnetotail, Plasma sheet, Neutral sheet

Introduction

The two magnetic hemispheres in the Earth's magnetotail are separated by a dawn-to-dusk-directed cross-tail current sheet. Within the current sheet, the boundary between the magnetic hemispheres is usually defined as a surface at which the X component (along the Sun–Earth line) of the tail magnetic field reverses ($B_x = 0$). It is called the neutral sheet (Ness 1965).

The position of the tail neutral sheet is often subjected to dynamical motion in the north–south Z direction termed as flapping (e.g., Speiser and Ness 1967; Lui et al. 1978; Sergeev et al. 1998, 2004; Zhang et al. 2002, 2005; Gao et al. 2018). In general, the position of the neutral sheet is affected by three major causes: hinging, warping and twisting (or rotation) (Tsyganenko et al. 1998; Tsyganenko and Fairfield 2004; Tsyganenko et al. 2015; Xiao et al. 2016, and references therein). The hinging effect shifts the neutral sheet northward and southward with respect to the Sun–Earth line when the geomagnetic dipole tilt angle is positive (generally northern hemisphere summer) and negative (northern hemisphere winter), respectively. The warping effect is also dependent on the dipole tilt angle: for positive dipole tilt angle, the warped neutral sheet appears in the tail cross-sectional plane as a southward opening curve (see e.g., Tsyganenko et al. 2015, their Figure 9). For negative dipole tilt angle, the warped neutral sheet opens northward. The twisting or rotation effect depends strongly on the dawn–dusk component of the interplanetary magnetic field (IMF B_y). For duskward, IMF $B_y > 0$, the neutral sheet is rotated counter-clockwise in the tail cross-sectional plane when looking from Earth toward the tail. For dawnward, IMF $B_y < 0$, the rotation is clockwise.

In one scenario, the rotation of the neutral sheet is caused by the following sequence of events: a non-zero IMF B_y drives an asymmetric magnetic reconnection on the dayside magnetopause. The magnetic tension force

*Correspondence: timo.pitkanen@space.umu.se
[1] Shandong Provincial Key Laboratory of Optical Astronomy and Solar-Terrestrial Environment, Institute of Space Sciences, Shandong University, Weihai, China
Full list of author information is available at the end of the article

deflects the newly opened field lines (southward IMF) or the field lines remaining open (northward IMF) to opposite dawn–dusk directions in the two hemispheres, which leads to an asymmetric accumulation of magnetic flux in the tail lobes (e.g., Tenfjord et al. 2015; Tenfjord et al. 2018). This generates an excess of magnetic pressure on the dawnside of one and duskside of the other tail lobe so that a torque is exerted on the plasma sheet. The magnetotail then reaches a new equilibrium state by rotating the plasma sheet as well as the neutral sheet. Also, it has been suggested that the tangential stress on the tail magnetopause by the deflecting open field lines exerts a torque on the lobes, which can subsequently lead to the rotation of the neutral sheet (Cowley 1981).

Several statistical studies suggest that the neutral sheet rotation increases with tailward distance from Earth as well as with increasing IMF B_y magnitude, and is generally stronger during northward compared to during southward IMF (Tsyganenko et al. 1998; Tsyganenko and Fairfield 2004; Tsyganenko et al. 2015). The same IMF B_y and B_z dependence of the neutral sheet rotation appears also in MHD simulations (e.g., Kullen and Janhunen 2004, and references therein).

While semi-empirical neutral sheet models (e.g., Tsyganenko et al. 2015) assume that the degree of the rotation is independent of the sign of IMF B_y, the statistical results by Kaymaz et al. (1994) and Owen et al. (1995) suggest a possibility that this would not be the case, although this is not explicitly discussed in their respective papers. Using IMP-8 magnetic field measurements in the range of $-40 < \mathrm{XGSM} < -25\ R_E$ (GSM, geocentric solar magnetospheric), Kaymaz et al. (1994) statistically inferred that the degree of the neutral sheet rotation in their dataset is slightly weaker for negative IMF B_y than for positive IMF B_y. Notably, the results by Kaymaz et al. (1994) showed signatures of nonlinear rotation, which weakens the inference of the rotation angle. Owen et al. (1995) investigated statistically the orientation of the edge of the plasma sheet boundary layer (PSBL) using particle measurements by ISEE-3 satellite from a large range of distances, between -240 and 0 R_E XGSM. They found that the average PSBL edge tilt angle was smaller for negative than for positive IMF B_y. Owen et al. (1995) concluded that the tail is generally more twisted around its axis for positive IMF B_y. However, their results show very large scattering in the individual PSBL edge tilt angles and the method gives only indirect evidence of the neutral sheet rotation.

Xiao et al. (2016), on the other hand, studied the average shape and position of the tail neutral sheet using data from multiple missions. They inferred that at low dipole tilt angles (absolute value less than 5°), the degree of the neutral sheet rotation was comparable for positive and negative IMF B_y, when the range of the IMF B_y magnitude was from 3 to 8 nT. Precisely taken, a slightly larger rotation was inferred for negative IMF B_y. When separating the northward and southward IMF, the difference between positive and negative IMF B_y in the rotation became clearer, but the characteristics of larger rotation for negative IMF B_y remained in both cases.

In this letter, we investigate possible asymmetric responses in the tail neutral sheet rotation to different IMF directions. In the analysis approach, which is based on the identification of the measured neutral sheet crossings, we make use of the neutral sheet model by Tsyganenko et al. (2015). A major advance compared to the study by Kaymaz et al. (1994) is that we distinguish positive and negative IMF B_z conditions. In addition, we distinguish small and large IMF B_y magnitudes, which has been done neither by Kaymaz et al. (1994) nor Xiao et al. (2016).

Data and methods

Data

We use magnetotail data from the Geotail, Time History of Events and Macroscale Interactions during Substorms (THEMIS) and Cluster missions. Geotail data consist of the spin-averaged (3 s) magnetic field measurements from the MaGnetic Field experiment (MGF) (Kokubun et al. 1994) and the 12-s ion moments from the Low Energy Particle experiment (LEP) (Mukai et al. 1994) measured over the years 1995–2006. The THEMIS data are the spin-averaged (3 s) magnetic field observations from the FluxGate Magnetometer (FGM) (Auster et al. 2008) and the ion moments computed onboard from the measurements by the ElectroStatic Analyzer (ESA) (McFadden et al. 2008). We use THEMIS data from the THEMIS-B and THEMIS-C satellites. For THEMIS-B the data coverage is from November 2007 till December 2009. THEMIS-C data cover August 2007–December 2009. From Cluster, we use spin-averaged (4 s) magnetic field measurements from the FluxGate Magnetometer (FGM) (Balogh et al. 2001) and the ion moments from the Hot Ion Analyzer (HIA) detector of the Cluster Ion Spectrometry (CIS) instrument (Rème et al. 2001) from the Cluster 3 spacecraft. The Cluster data cover the years 2001–2009.

For the solar wind data, we use the 1-min OMNI data propagated to the nominal bow shock nose (http://omniweb.gsfc.nasa.gov/) (King and Papitashvili 2005). In addition, we use 1-min SYM-H geomagnetic index data provided by the World Data Center for Geomagnetism, Kyoto, Japan, which are also retrieved through the OMNI database. The geocentric solar magnetospheric (GSM) coordinate system is used for all spacecraft data throughout the study.

Tsyganenko et al. (2015) neutral sheet model

In this study, we have utilized the semi-empirical neutral sheet model by Tsyganenko et al. (2015), hereafter denoted as the T15 neutral sheet model. Here, we briefly present the main features of the model. For a detailed description, the reader is referred to Tsyganenko et al. (2015).

The T15 model describes the global shape of the unperturbed magnetospheric equatorial current sheet (neutral sheet) at all local times as a function of geomagnetic dipole tilt angle (Ψ), solar wind dynamic pressure (P_{dyn}), IMF B_y and IMF B_z. It has been derived from a vast data pool of magnetic field measurements from Polar, Cluster, Geotail and THEMIS missions between 1995 and 2013.

In the solar magnetic (SM) cylindrical coordinates, the position of the model neutral sheet in the Z axis, Z_s, is determined by the form

$$Z_s = R_H \tan\Psi \left\{ 1 - \left[1 + \left(\frac{\rho}{R_H} \right)^{\alpha} \right]^{1/\alpha} \right\} \times \left(a_0 + a_1 \cos\phi \right) + T \frac{B_y}{B_{y0}} \left(\frac{\rho}{\rho_0} \right)^{\beta} \sin\phi. \quad (1)$$

The first two terms describe the hinging and warping and the last third term determines the rotation of the neutral sheet. In the formula R_H is the hinging distance, which depends on P_{dyn}, IMF B_z and the longitude ϕ for which $\tan\phi = Y/X$. Ψ is the dipole tilt angle, $\rho = \sqrt{X^2 + Y^2}$, a_0 and a_1 are Fourier coefficients, which depend on P_{dyn} and IMF B_z. The magnitude coefficient T depends on P_{dyn} and the power index α depends on ϕ, P_{dyn} and IMF B_z. The power index β depends only on IMF B_z. $B_{y0} = 5$ nT and $\rho_0 = 10R_E$ are numerical scaling factors.

The source code (Fortran) for the T15 neutral sheet model with input and output in GSM coordinates is provided at http://geo.phys.spbu.ru/~tsyganenko/modeling.html.

Methods

We have statistically investigated the rotation of the neutral sheet. Our approach is based on the identification of the neutral sheet positions and an investigation of their distribution. To identify the positions of the neutral sheet crossings in the magnetotail plasma sheet from the data, we have utilized the following procedure. First, the magnetospheric data were averaged to a 5-min time resolution. Small data gaps were allowed so that > 80% (= 4 min) of data must be available. For the data point to be included in the database, we required average plasma ion $\beta \geq 0.1$ for the 5-min interval. The threshold for ion β, which is the ratio between ion thermal pressure and magnetic pressure, was used to exclude measurements from the low-β lobes. Then, we identified the neutral sheet crossings in the tail region $-30 <$ XGSM $< -15R_{\mathrm{E}}$ and $-25 <$ YGSM $< +25R_{\mathrm{E}}$ as reversals in the magnetic field B_x component in the 5-min data. The tail range of $-30 <$ XGSM $< -15R_{\mathrm{E}}$ was chosen to only include clearly tail-like distances and it is limited in the far side by the apogees of the satellite trajectories.

A crossing was accepted to the neutral sheet crossing dataset if the following conditions were fulfilled: (1) the ion speed $V_{\perp xy} = \sqrt{V_{\perp x}^2 + V_{\perp y}^2} < 100$ km/s in the XY plane for the 5-min data samples right before and after the crossing. This is expected to efficiently remove high-speed flows, which can perturb the neutral sheet, and tailward magnetosheath flows in the magnetotail flanks from the dataset. (2) The IMF magnitude $B < 10$ nT, the solar wind dynamic pressure $0.1 \leq P_{dyn} \leq 10$ nPa and $-100 \leq$ SYM-H ≤ 30 nT (Tsyganenko et al. 2015). Thus, the most extreme solar wind and magnetospheric conditions were excluded. IMF **B** was computed as a 40-min average over a time interval from 35 min prior to the neutral sheet crossing until 5 min after the crossing. This the same averaging window used by Tsyganenko et al. (2015). Notably, Case et al. (2018) suggest a time scale of 10–20 min for the response of the neutral sheet to the IMF B_y reversals, which is within the averaging window of Tsyganenko et al. (2015) and the present study. P_{dyn} and SYM-H were computed as averages over the 10-min period centered at the crossing. Tsyganenko et al. (2015) used a 5-min average and the instantaneous 1-min value for P_{dyn} and SYM-H, respectively. We argue that 10-min averages describe better the general conditions around the crossing times. In the computation of IMF **B** and P_{dyn}, total missing data up to 30% in the averaging time intervals were allowed. (3) The measured neutral sheet crossing position differs no more than 4 R_{E} in the ZGSM direction from the model neutral sheet by Tsyganenko et al. (2015). This removes outliers caused by the most extreme neutral sheet perturbations from the dataset in the same way as has been done in the study by Tsyganenko et al. (2015).

In total, 2963 neutral sheet crossings were obtained for the dataset. Using the T15 neutral sheet model, we removed the contributions of the hinging and warping to the position for each neutral sheet crossing in this dataset. This was done by computing a new neutral sheet ZGSM position using the T15 model (equation (1)) without the rotation term, i.e., without the last term of equation (1), and subtracting the result from the observed ZGSM position for each data point of the dataset. As a result, one gets an estimate for the neutral sheet ZGSM position caused by the rotation effect only (referred to as dataset O). When using the T15 neutral sheet model in this study, we assume that it represents the nominal neutral sheet position in the absence of perturbations, such as north–south flappings. As input for the T15 model, IMF and P_{dyn} values were used that are averaged in the same way as described above. For comparison, we also computed the T15 model neutral sheet ZGSM positions caused by the rotation effect only. This was done by subtracting the T15 model neutral sheet ZGSM position computed without rotation from the full T15 model, which is equivalent to computing the ZGSM position with the T15 rotation term only (referred to as dataset M). In the computation, the XGSM and YGSM positions and the IMF and P_{dyn} that are associated with the actual measured neutral sheet crossings were used.

We sorted the neutral sheet crossings in eight different categories: those observed during northward and southward IMF conditions and further, those with positive and negative IMF B_y with large (> 3 nT) and small (0 < IMF B_y < 3 nT) magnitudes. Then we investigated the degree of the rotation in each of the categories in the two datasets M (model) and O (observations). The locations of the neutral sheet crossings in each category projected to the GSM XY plane are shown in Fig. 1. The relative numbers of the removed outliers in each IMF category varied between 1 and 9% of the numbers of the included neutral sheet crossings.

Results

Figure 2 displays the results for the northward IMF conditions (IMF $B_z > 0$), for dataset M (T15 model) on the left panels and for dataset O (Data) on the right panels. Shown are the positions of the neutral sheet crossings in the GSM YZ plane for each IMF category (when looking from Earth tailward). In each category, we have fitted a line of best fit of linear least squares sense to the data points to statistically estimate the neutral sheet rotation. The rotation is measured by the angle α between the YGSM axis and the regression line and it is increasing anti-clockwise from the positive YGSM axis. The angle α is computed as a gradient of the best-fitted line. The given error estimate for α is the standard error. Note that in the T15 model, the curve describing the neutral sheet in each tail cross-sectional plane due to the rotation, is precisely taken nonlinear. This is because the rotation term in the T15 model is dependent on the sinus of the longitude ϕ, i.e., the rotation in one tail cross-section increases towards the flanks (see equation (1) and Tsyganenko et al. 2015, their Figure 10). A linear fit is, however, sufficient for our purpose, since we are interested in quantifying the degree of the rotation at general level.

By intercomparing the model results (dataset M, Fig. 2a,c,e,g), we see that the degree of the rotation ($|\alpha|$) is clearly a few degrees larger for large than for small IMF B_y magnitudes. This is expected, as the rotation angle in the T15 model depends, among other parameters, on the magnitude of IMF B_y. The magnitude of the angle α is also slightly larger for positive IMF B_y compared to negative IMF B_y. But in general, the degrees of the rotation are comparable between the two IMF B_y signs. Since the T15 neutral sheet model does not distinguish between positive and negative IMF B_y in the degree of the rotation, this means that any differences seen in the model dataset M for positive and negative IMF B_y can only come from the differences in the distributions of the model input parameters and the XY positions of the neutral sheet crossings.

The magnitude of the rotation angle increases with the distance in the X direction in the T15 neutral sheet model (Tsyganenko et al. 2015). However, the scatter of the modeled data points from the regression line in each category are small, as also indicated by the high r-squared values. Therefore, we conclude that the distributions of the crossings in XGSM (Fig. 1) do not affect the determination of the rotation angle.

When looking at the observations (dataset O, Fig. 2b, d, f, h), the scattering of the data points with respect to the regression line is significantly larger if compared to the model. This is understandable, because other effects such as flapping contribute to the measured positions of the neutral sheet. In the model, these effects are absent. Generally, the magnitudes of the rotation angles are smaller for the data than for the model, except for low-magnitude positive IMF B_y (Fig. 2f).

The striking difference between the data (dataset O) and the model (dataset M) is the strong rotation asymmetry between positive and negative IMF B_y in dataset O. For the model (dataset M), $|\alpha|$ for positive and negative IMF B_y are comparable, both in the case of large (Fig. 2a and c) and small IMF B_y magnitudes (Fig. 2e and g). For the data (dataset O), for large IMF B_y magnitudes (Fig. 2b and d), $|\alpha|$ is clearly smaller for negative IMF B_y, $1.80 \pm 0.39°$, compared to $5.48 \pm 0.30°$ for positive IMF B_y. For small IMF B_y magnitudes, a clear rotation can be deduced for positive IMF B_y ($4.17 \pm 0.25°$, Fig. 2f), but no significant rotation for negative IMF B_y ($0.25 \pm 0.29°$, Fig. 2h). In fact, in the latter case the sense of the rotation is in an unexpected direction ($\alpha > 0$), but the rotation angle stays within the error limits.

Figure 3 displays the results for the southward IMF (IMF $B_z < 0$). From the model results (dataset M), we see that similar to the northward IMF, the degree of the rotation is a couple of degrees larger for large than for small IMF B_y magnitudes (Fig. 3a,c,e,g). For large IMF B_y magnitudes, $|\alpha|$ is almost the same for positive and negative IMF B_y (Fig. 3a and c). For small IMF B_y magnitudes, $|\alpha|$ is slightly larger for positive IMF B_y but still comparable (Fig. 3e and g).

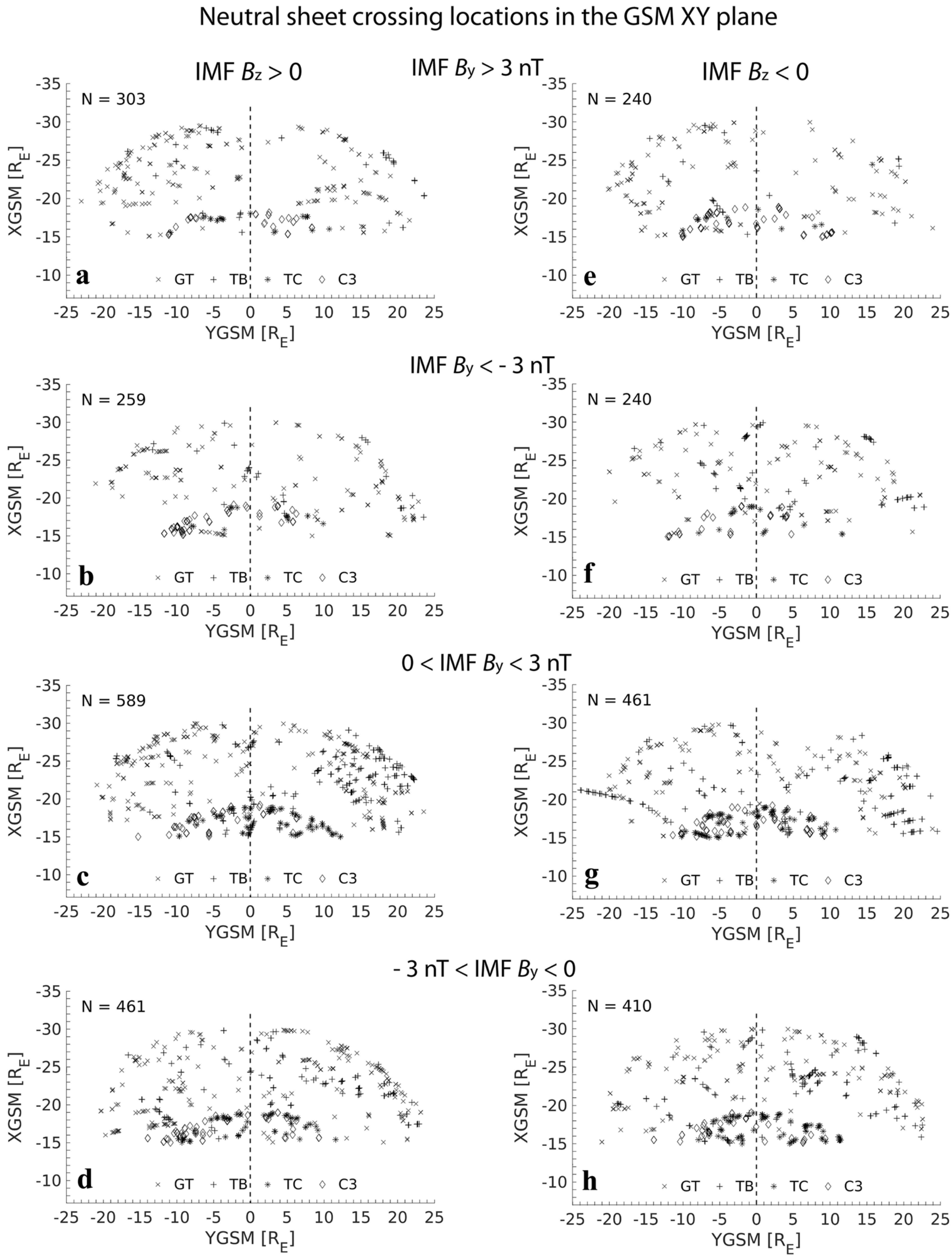

Fig. 1 Locations of the neutral sheet crossings in the GSM XY plane for the different IMF categories

When looking at the observations (Fig. 3b, d, f, h), we again observe large differences in $|\alpha|$ between positive and negative IMF B_y as in the case of the northward IMF. At large IMF B_y magnitudes, a clear rotation can be seen for positive IMF B_y ($2.85 \pm 0.30°$, Fig. 3b), but no significant rotation for negative IMF B_y ($0.27 \pm 0.39°$, Fig. 3d). In the latter case, the rotation angle is slightly positive, i.e., in the unexpected direction, but within the error limits. At small IMF B_y magnitudes, similarly, a clear rotation appears for positive IMF B_y ($2.68 \pm 0.21°$, Fig. 3f) (which notably has larger α than the model, Fig. 3e). But contrary to what are expected, the rotation angle for negative IMF B_y is clearly opposite, positive ($1.26 \pm 0.28°$, Fig. 3h).

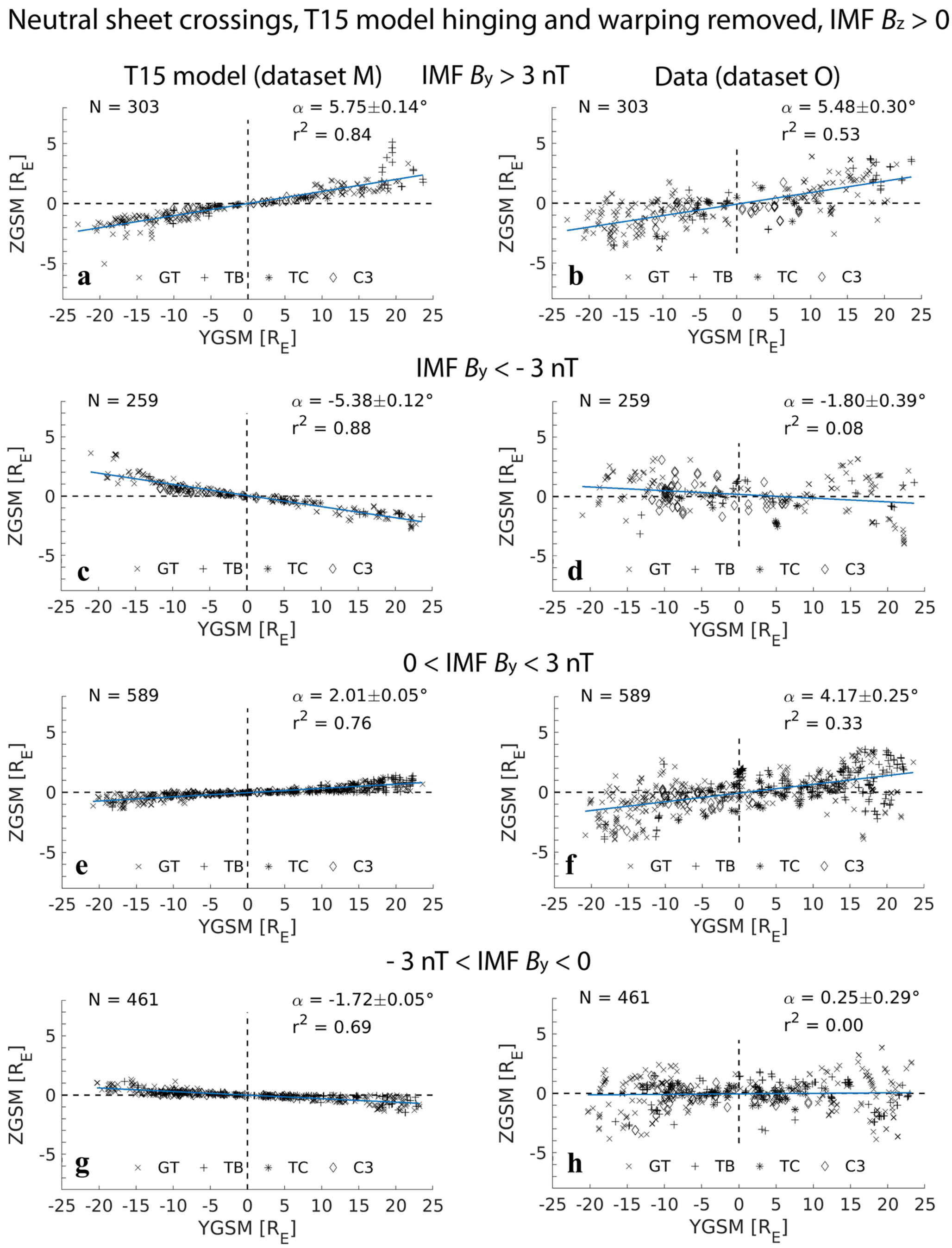

Fig. 2 Locations of the neutral sheet crossings in the GSM YZ plane for IMF $B_z > 0$ conditions and different IMF B_y conditions after removal of the hinging and warping effects according to the T15 neutral sheet model. Left: T15 model (dataset M). Right: data (dataset O). GT = Geotail, TB = THEMIS-B, TC = THEMIS-C and C3 = Cluster 3. In each panel, *N* marks the number of the neutral sheet crossings, the blue line a linear regression and the angle α the angle between the YGSM axis and the regression line indicating the rotation of the neutral sheet (increases from the positive YGSM axis toward the positive ZGSM axis). r^2 is the quality indicator of the regression (square of the Pearson's correlation coefficient). The ZGSM scale has been zoomed in to magnify the rotation

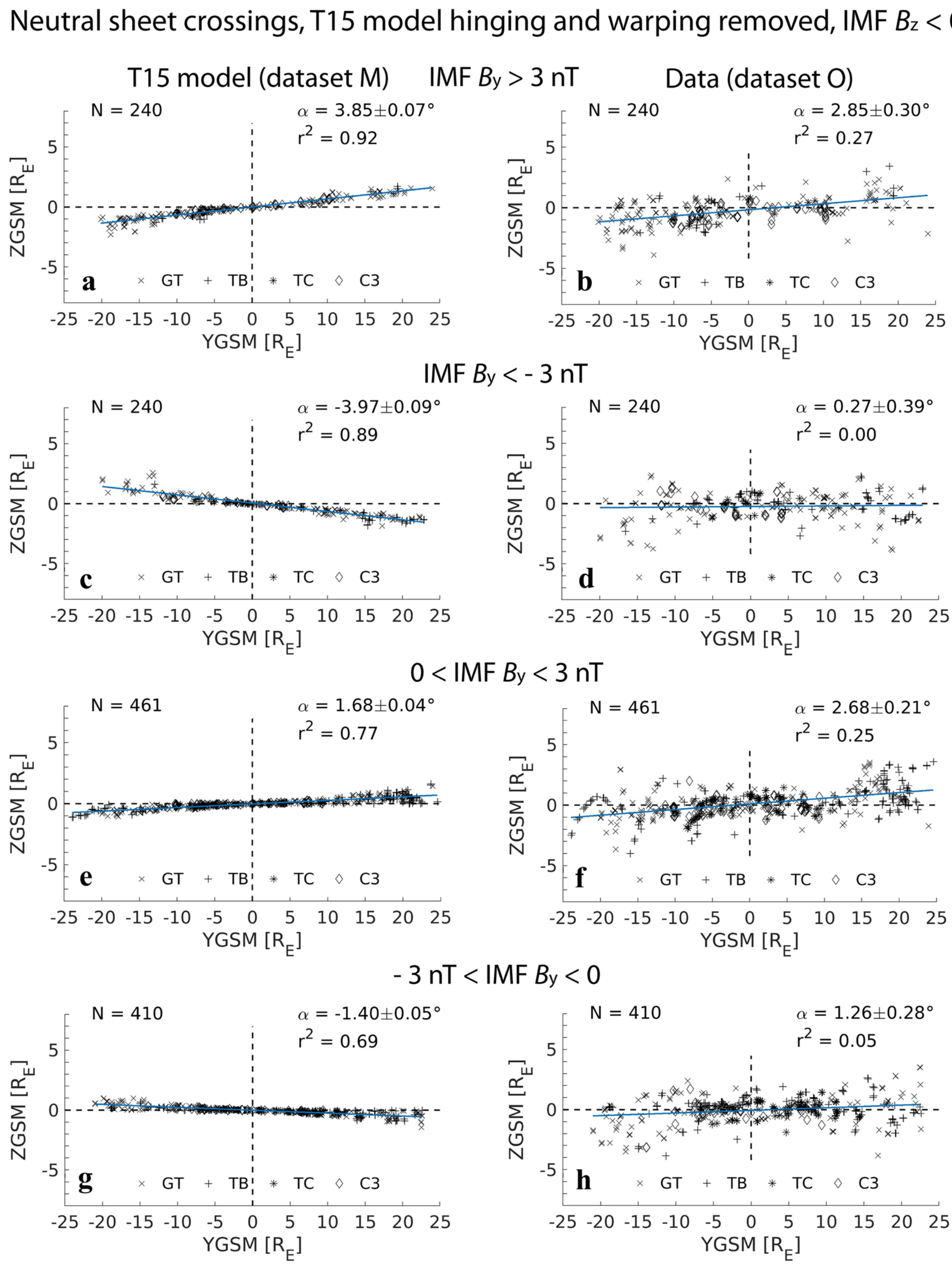

Fig. 3 Same as Fig. 2, but for IMF $B_z < 0$

Generally, the degree of the neutral sheet rotation is larger for northward than southward IMF conditions, which is consistent with previous studies (e.g., Owen et al. 1995; Tsyganenko et al. 2015).

Discussion

The observational results (dataset O) presented in Figs. 2 and 3 indicate differences in the degree of the neutral sheet rotation between positive and negative IMF B_y

conditions. Comparison to the model (dataset M) implies that these differences are so large that they cannot be explained by the distributions of model input parameters and spatial XY positions of the neutral sheet crossings.

The tail neutral sheet crossings are generally measured when the neutral sheet moves fast, i.e., flaps in the north–south direction and passes the satellite position rather than the satellite moves across a static neutral sheet. From the large scattering of the crossings in dataset O, it is clear that the flapping affects the estimates of the rotation angle. However, it has been deduced that the typical amplitudes of the flapping motion are on the order of 1–2 R_E (Sergeev et al. 2006). Because we obtain a clear positive rotation angle α for positive IMF B_y in all categories, we argue that the scattering caused by the flapping cannot explain (i) the small magnitude of negative α in Fig. 2d, (ii) the very small opposite rotation in Figs. 2h and 3d, and (iii) the clear opposite rotation direction in Fig. 3h, for negative IMF B_y (the rotation is counterclockwise as for positive IMF B_y while clockwise rotation is expected for negative IMF B_y). It might explain the difference, if flapping would be more significant for negative IMF B_y, but this is fully speculative.

Another cause for the scattering could arise from the response of the neutral sheet to IMF B_y reversals (Case et al. 2018). Assume that a neutral sheet crossing is detected in the dusk and ZGSM > 0 quadrant in the YZ plane when IMF $B_y > 0$ has been prevailing for a longer time. The crossing is detected either as the neutral sheet flaps or the positive rotation increases. The crossing is thus observed in the expected quadrant in the corresponding IMF $B_y > 0$ category (the expected quadrant is the quadrant one expects the neutral sheet to rotate into, based on the prevailing IMF B_y conditions). Then IMF B_y suddenly reverses to IMF $B_y < 0$, and a second crossing is detected if the neutral sheet responds to the IMF B_y reversal and rotates to a new (opposite) angle corresponding to the IMF $B_y < 0$ condition. If this would happen, this second crossing would still be observed in the quadrant, which is in accordance with the IMF $B_y >$ 0 condition (dusk and ZGSM > 0) because the satellite position practically remains unchanged. If the separation of the crossing times were long enough, the averaged IMF B_y value would be negative and the crossing would appear in the unexpected quadrant for IMF $B_y < 0$. This would subsequently increase the scattering in the corresponding IMF $B_y < 0$ category.

We have investigated the possible influence of IMF B_y reversals occurring prior to the crossings on the results. We computed ∼ 1-h average (60 min prior to until 5 min after a crossing) of IMF and compared this 1-h IMF B_y direction to the assigned (35 min prior to until 5 min after a crossing) IMF B_y direction. One can assume that if these are collinear, no significant reversal took place. We find that for the categories of large IMF B_y magnitudes, there appear only 0–2 neutral sheet crossings in each category for which the 1-h IMF B_y direction is opposite to the assigned IMF B_y direction. Thus, IMF B_y reversals do not affect the results in these categories. In the case of small magnitude IMF B_y categories, the relative number of the IMF B_y reversal crossings vary from 5 to 12% and the effects to the neutral sheet rotation angle are small, 4–5%, except for northward IMF B_z and $-3 <$ IMF $B_y < 0$ nT-category (Fig. 2h). While in this category, the contribution of the neutral sheet crossings associated with the IMF B_y reversal leads to a relatively high increase of the rotation angle to the unexpected direction, in percentage ∼733%, the absolute increase in the angle is only 0.22° (from 0.03° to 0.25°). All the deviations in the neutral sheet rotation angle caused by the IMF B_y reversals are within the error limits. Therefore, we argue that IMF B_y reversals cannot explain the large differences in the degree of the rotation.

The distributions of the IMF B_y magnitudes inside each category could also affect the results. If the distribution of the IMF B_y magnitudes would be biased

Table 1 Mean and median of IMF B_y and IMF B_z tagged to the neutral sheet crossings in each of the IMF categories (in nT)

IMF $B_z > 0$	Mean IMF B_y	Median IMF B_y	Mean IMF B_z	Median IMF B_z
IMF $B_y > 3$ nT	4.5	4.2	2.2	1.7
IMF $B_y < -3$ nT	− 4.6	− 4.2	2.2	1.7
$0 <$ IMF $B_y < 3$ nT	1.4	1.4	1.8	1.4
-3 nT $<$ IMF $B_y < 0$	− 1.5	− 1.5	1.6	1.3
IMF $B_z < 0$	**Mean IMF B_y**	**Median IMF B_y**	**Mean IMF B_z**	**Median IMF B_z**
IMF $B_y > 3$ nT	4.5	4.0	− 1.7	− 1.5
IMF $B_y < -3$ nT	− 4.4	− 3.9	− 1.9	− 1.7
$0 <$ IMF $B_y < 3$ nT	1.6	1.6	− 1.3	− 1.0
-3 nT $<$ IMF $B_y < 0$	− 1.5	− 1.5	− 1.6	− 1.1

toward larger magnitudes for positive and toward smaller magnitudes for negative IMF B_y, that might explain at least partly the larger degree of the rotation for positive IMF B_y. However, by comparing the distributions for positive and negative IMF B_y, we do not find any significant differences between them and thus exclude that as the potential cause. The mean and median of IMF B_y (and IMF B_z) in each IMF category are shown in Table 1.

The observational results that the degree of the neutral sheet rotation is larger for positive IMF B_y are in accordance with the results by Kaymaz et al. (1994). Notably, Kaymaz et al. (1994) found in their dataset a quite clear rotation also for negative IMF B_y, whereas in our dataset the rotation is clear and in the expected direction for negative IMF B_y only for northward IMF and IMF $B_y < -3$ nT (Fig. 2d). In their dataset, Kaymaz et al. (1994) used only data for which IMF $|B_y| > |B_z|$ and did not distinguish between northward and southward IMF. We have checked subsets of data using the same condition, but the differences in the results are relatively small. The rotation angles (without error estimates, which have the similar magnitudes as in Figs. 2 and 3) in the same order as the IMF B_y categories in Figs. 2 and 3 are for northward IMF B_z: 5.28°, −2.32°, 4.70° and 0.02°. For southward IMF B_z the rotation angles are: 2.81°, 0.20°, 3.04° and 1.26°.

Owen et al. (1995) found that the average PSBL edge tilt angle was smaller for negative than positive IMF B_y. Owen et al. (1995) further distinguished northward and southward IMF B_z and found that the magnitudes of the PSBL tilt angles were clearly larger for northward than southward IMF. If one assumes that the PSBL tilt angle reflects the rotation of the neutral sheet, our results agree with this aspect with the results by Owen et al. (1995). Also, the T15 neutral sheet model gives larger rotation for northward than for southward IMF, but it does not distinguish between positive and negative IMF B_y (Tsyganenko et al. 2015).

The results that the rotation of the neutral sheet is weaker for negative than for positive IMF B_y raises a question of a possible intrinsic degree of the rotation when IMF $B_y = 0$. In a hypothetical scenario, the tail neutral sheet is always slightly rotated with a small positive α under zero IMF B_y condition. Therefore, one would need a small negative IMF B_y to rotate α to zero. However, the results by Xiao et al. (2016) do not support this scenario. Xiao et al. (2016) also studied the neutral sheet rotation at low dipole tilt angles for $-1 <$ IMF $B_y < 1$ nT, so approximately for zero IMF B_y. They found no indication of intrinsic rotation. Furthermore, Xiao et al. (2016) found a slightly larger rotation for clearly negative IMF B_y ($-8 <$ IMF $B_y < -3$ nT) than for clearly positive IMF B_y ($3 <$ IMF $B_y < 8$ nT). This is not in accordance with the results of the present study and with the results by Kaymaz et al. (1994) and Owen et al. (1995).

The differences in the results, specifically between the present study (larger rotation for positive IMF B_y) and the study by Xiao et al. (2016) (larger rotation for negative IMF B_y) are difficult to explain. The two studies use data from approximately similar time intervals for almost the same satellites, although Xiao et al. (2016) are using more data with one additional mission, TC-1 (Carr et al. 2005).

The difference could arise from the different methods used. In our method, the individual neutral sheet crossings are identified and the T15 neutral sheet model is used to remove the hinging and warping effects from the neutral sheet positions. Then a line is fitted to the datapoints in the YZ plane to extract the rotation. In the Xiao et al. (2016) method, tail B_x measurements are binned to squares in the YZ plane and the majority of the B_x measurement samples in a bin determines whether the bin is assigned by positive or negative B_x bin. A line is then fitted to the position points that separate the positive and negative B_x regions to get the rotation angle. This is done for the data with low dipole tilt angles (absolute value less than 5°) to minimize the hinging and warping. We have checked the neutral sheet rotation in each IMF category for a subset of our dataset using the same range for the low dipole tilt angle as Xiao et al. (2016). While the number of neutral sheet crossings in each category are much smaller indicating weaker statistics, the asymmetry between the positive and negative IMF B_y remains (data not shown).

Our method is likely to have larger scattering of the datapoints that construct the fit, because all the datapoints in the particular IMF category are included in the fit. While not explicitly stated by Xiao et al. (2016), we assume that in the method by Xiao et al. (2016), only the position data assigned by white color (in their Figures 10 and 11) are included in the fit. This means that for each spatial Y bin, only one position is taken to the fitting process, and the scattering of these datapoints is generally much smaller. However, generally, the scattering from the fitted line in our method does not vary significantly between the IMF B_y categories (Figs. 2 and 3).

The difference in the degree of the neutral sheet rotation could be caused by differences in the asymmetric accumulation of magnetic flux into the tail lobes in case the accumulation would not be an exact mirror process for positive and negative IMF B_y. It is also possible that there exists another still unidentified mechanism that is more efficient under one IMF B_y direction. These questions require further investigation. As a future work, the influence of IMF B_y on the neutral sheet rotation should be studied using numerical global magnetosphere models. It should be tested whether the present models produce the difference in the degree of the rotation between positive and negative IMF B_y, and if yes, then investigated the physical process(es) behind the asymmetry.

Summary

We have used Geotail, THEMIS and Cluster data from 1995 to 2009 to statistically investigate the rotation of the neutral sheet under the influence of non-zero IMF B_y in the Earth's magnetotail. With help of T15 neutral sheet model (Tsyganenko et al. 2015), we find in the tail range of $-30 < \text{XGSM} < -15\ R_E$, the degree of the neutral sheet rotation is clearly smaller, there appears no significant rotation or the rotation is even clearly in an opposite direction to what is expected for negative IMF B_y compared to positive IMF B_y. For positive IMF B_y, the inferred rotation angle varies between 2.68° and 5.48° and for negative IMF B_y, the rotation angle gets values from −1.80° to 1.26°. A comparison to the T15 model suggests that this asymmetry in the neutral sheet rotation between positive and negative IMF B_y conditions is too large to be explained only by an uneven distribution of the neutral sheet crossings or other solar wind conditions at the observed neutral sheet crossings, which have been deduced to contribute to the position of the neutral sheet.

The possible physical mechanism remains unclear. The discrepancy between the results from different studies indicate that more research is needed to understand the IMF B_y influence on the rotation of the neutral sheet. Different approaches are desired to find out all related aspects. While numerical modeling, such as global magnetosphere models, can be used in investigations, they cannot replace observational studies. Based on the results of the present study, we suggest that in the future, magnetospheric models such as semi-empirical neutral sheet models, should be parameterized so that asymmetric effects due to the IMF B_y direction are allowed for.

The asymmetries related to the IMF B_y sign are not limited to the neutral sheet rotation. Recent studies have found IMF B_y sign-related asymmetries for instance in the high-latitude geomagnetic activity (Holappa and Mursula 2018) and in the polar cap size (Reistad et al. 2020).

Acknowledgements
The authors thank the Geotail mission PI, Geotail LEP and MGF instrument PIs and teams for the Geotail data, and the THEMIS FGM, ESA and SST instrument PIs and teams as well as the PI of the THEMIS mission for the THEMIS data. In addition, we thank the Cluster mission PI, Cluster CIS and FGM instrument PIs and teams for the Cluster data. Furthermore, we acknowledge GSFC SPDF/OMNIWeb and WDC for Geomagnetism, Kyoto, Japan, for the solar wind and SYM-H index data.

Authors' contributions
TP was responsible for the data analysis and drafting the manuscript. AK, LC, J-SP and HV contributed to the data analysis. All authors contributed to the interpretation of the results and/or drafting the manuscript. All authors read and approved the final manuscript.

Funding
The work was supported by the Swedish National Space Agency (SNSA) Grants 118/17 (T.P. and A.K.), 105/14 (A.D.S.), 81/17 (G.S.C.) and 271/14 (M.H.), the National Natural Science Foundation of China (NSFC) Grants 41750110486 (T.P.) and 41850410495 (J.-S.P.) and the Academy of Finland Grant 314664 (H.V.).

Availability of data and materials
The Geotail and THEMIS data were accessed through https://cdaweb.sci.gsfc.nasa.gov/index.html/. The Cluster data were accessed through https://www.cosmos.esa.int/web/csa. The solar wind and SYM-H index data are available through http://omniweb.gsfc.nasa.gov/. The source codes (Fortran) for the Geopack 08 and the T15 neutral sheet model used in the data analysis are provided at http://geo.phys.spbu.ru/~tsyganenko/modeling.html

Competing interests
The authors declare that they have no competing interests.

Author details
[1] Shandong Provincial Key Laboratory of Optical Astronomy and Solar-Terrestrial Environment, Institute of Space Sciences, Shandong University, Weihai, China. [2] Department of Physics, Umeå University, Umeå, Sweden. [3] Space Physics and Astronomy Research Unit, University of Oulu, Oulu, Finland. [4] Space and Plasma Physics, School of Electrical Engineering and Computer Science, Royal Institute of Technology, Stockholm, Sweden.

Received: 5 October 2020 Accepted: 15 December 2020
Published online: 12 January 2021

References

Auster HU, Glassmeier KH, Magnes W, Aydogar O, Baumjohann W, Constantinescu D, Fischer D, Fornacon KH, Georgescu E, Harvey P, Hillenmaier O, Kroth R, Ludlam M, Narita Y, Nakamura R, Okrafka K, Plaschke F, Richter I, Schwarzl H, Stoll B, Valavanoglou A, Wiedemann M (2008) The THEMIS fluxgate magnetometer. Space Sci Rev 141:235–264. https://doi.org/10.1007/s11214-008-9365-9

Balogh A, Carr CM, Acuña MH, Dunlop MW, Beek TJ, Brown P, Fornaçon K-H, Georgescu E, Glassmeier K-H, Harris J, Musmann G, Oddy T, Schwingenschuh K (2001) The cluster magnetic field investigation: overview of in-flight performance and initial results. Annales Geophysicae 19:1207–1217. https://doi.org/10.5194/angeo-19-1207-2001

Carr C, Brown P, Zhang TL, Gloag J, Horbury T, Lucek E, Magnes W, O'Brien H, Oddy T, Auster U, Austin P, Aydogar O, Balogh A, Baumjohann W, Beek T, Eichelberger H, Fornacon K-H, Georgescu E, Glassmeier K-H, Ludlam M, Nakamura R, Richter I (2005) The Double Star magnetic field investigation: instrument design, performance and highlights of the first year's observations. Annales Geophysicae 23(8):2713–2732. https://doi.org/10.5194/angeo-23-2713-2005

Case NA, Grocott A, Haaland S, Martin CJ, Nagai T (2018) Response of Earth's Neutral Sheet to Reversals in the IMF B_y Component. J Geophys Res Space Phys 123:8206–8218. https://doi.org/10.1029/2018JA025712

Cowley SWH (1981) Magnetospheric asymmetries associated with the y-component of the IMF. Planet Space Sci 29(1):79–96. https://doi.org/10.1016/0032-0633(81)90141-0

Gao JW, Rong ZJ, Cai YH, Lui ATY, Petrukovich AA, Shen C, Dunlop MW, Wei Y, Wan WX (2018) The distribution of two flapping types of magnetotail current sheet: implication for the flapping mechanism. J Geophys Res Space Phys 123:7413–7423. https://doi.org/10.1029/2018JA025695

Holappa L, Mursula K (2018) Explicit IMF B_y Dependence in High-Latitude Geomagnetic Activity. J Geophys Res Space Phys 123(6):4728–4740. https://doi.org/10.1029/2018JA025517. **arXiv:1805.10699**.

Kaymaz Z, Siscoe GL, Luhmann JG, Lepping RP, Russell CT (1994) Interplanetary magnetic field control of magnetotail magnetic field geometry: IMP 8 observations. J Geophys Res 99:11113–11126. https://doi.org/10.1029/94JA00300

King JH, Papitashvili NE (2005) Solar wind spatial scales in and comparisons of hourly Wind and ACE plasma and magnetic field data. J Geophys Res 110(A2):02104. https://doi.org/10.1029/2004JA010649

Kokubun S, Yamamoto T, Acuña MH, Hayashi K, Shiokawa K, Kawano H (1994) The GEOTAIL magnetic field experiment. J Geomagn Geoelectr 46:7–21. https://doi.org/10.5636/jgg.46.7

Kullen A, Janhunen P (2004) Relation of polar auroral arcs to magnetotail twisting and IMF rotation: a systematic MHD simulation study. Annales Geophysicae 22:951–970. https://doi.org/10.1007/s11214-008-9365-91

Lui ATY, Meng C-I, Akasofu S-I (1978) Wavy nature of the magnetotail neutral sheet. Geophys Res Lett 5:279–282. https://doi.org/10.1029/GL005i004p00279

McFadden JP, Carlson CW, Larson D, Ludlam M, Abiad R, Elliott B, Turin P, Marckwordt M, Angelopoulos V (2008) The THEMIS ESA Plasma Instrument and In-flight Calibration. Space Sci Rev 141:277–302. https://doi.org/10.1007/s11214-008-9440-2

Mukai T, Machida S, Saito Y, Hirahara M, Terasawa T, Kaya N, Obara T, Ejiri M, Nishida A (1994) The low energy particle (LEP) experlment onboard the GEOTAIL satellite. J Geomagn Geoelectr 46:669–692. https://doi.org/10.5636/jgg.46.669

Ness NF (1965) The Earth's magnetic tail. J Geophys Res 70(13):2989–3005. https://doi.org/10.1029/JZ070i013p02989

Owen CJ, Slavin JA, Richardson IG, Murphy N, Hynds RJ (1995) Average motion, structure and orientation of the distant magnetotail determined from remote sensing of the edge of the plasma sheet boundary layer with E greater than 35 keV ions. J Geophys Res Space Phys 100:185–204. https://doi.org/10.1029/94JA02417

Reistad JP, Laundal KM, Ohma A, Moretto T, Milan SE (2020) An Explicit IMF B_y Dependence on Solar Wind-Magnetosphere Coupling. Geophys Res Lett 47(1):86062. https://doi.org/10.1029/2019GL086062

Rème H, Aoustin C, Bosqued JM, Dandouras I, Lavraud B, Sauvaud JA, Barthe A, Bouyssou J, Camus T, Coeur-Joly O, Cros A, Cuvilo J, Ducay F, Garbarowitz Y, Medale JL, Penou E, Perrier H, Romefort D, Rouzaud J, Vallat C, Alcaydé D, Jacquey C, Mazelle C, D'Uston C, Möbius E, Kistler LM, Crocker K, Granoff M, Mouikis C, Popecki M, Vosbury M, Klecker B, Hovestadt D, Kucharek H, Kuenneth E, Paschmann G, Scholer M, Sckopke N, Seidenschwang E, Carlson CW, Curtis DW, Ingraham C, Lin RP, McFadden JP, Parks GK, Phan T, Formisano V, Amata E, Bavassano-Cattaneo MB, Baldetti P, Bruno R, Chionchio G, di Lellis A, Marcucci MF, Pallocchia G, Korth A, Daly PW, Graeve B, Rosenbauer H, Vasyliunas V, McCarthy M, Wilber M, Eliasson L, Lundin R, Olsen S, Shelley EG, Fuselier S, Ghielmetti AG, Lennartsson W, Escoubet CP, Balsiger H, Friedel R, Cao J-B, Kovrazhkin RA, Papamastorakis I, Pellat R, Scudder J, Sonnerup B (2001) First multispacecraft ion measurements in and near the Earth's magnetosphere with the identical Cluster ion spectrometry (CIS) experiment. Annales Geophysicae 19:1303–1354. https://doi.org/10.5194/angeo-19-1207-20019

Sergeev V, Angelopoulos V, Carlson C, Sutcliffe P (1998) Current sheet measurements within a flapping plasma sheet. J Geophys Res 103:9177–9188. https://doi.org/10.1029/97JA02093

Sergeev V, Runov A, Baumjohann W, Nakamura R, Zhang TL, Balogh A, Louarnd P, Sauvaud J-A, Reme H (2004) Orientation and propagation of current sheet oscillations. Geophys Res Lett 31:05807. https://doi.org/10.1029/2003GL019346

Sergeev V, Sormakov DA, Apatenkov SV, Baumjohann W, Nakamura R, Runov AV, Mukai T, Nagai T (2006) Survey of large-amplitude flapping motions in the midtail current sheet. Annales Geophysicae 24:2015–2024. https://doi.org/10.5194/angeo-19-1207-20012

Speiser TW, Ness NF (1967) The neutral sheet in the geomagnetic tail: Its motion, equivalent currents, and field line connection through it. J Geophys Res 72(1):131–141. https://doi.org/10.1029/JZ072i001p00131

Tenfjord P, Østgaard N, Snekvik K, Laundal KM, Reistad JP, Haaland S, Milan SE (2015) How the IMF B_y induces a B_y component in the closed magnetosphere and how it leads to asymmetric currents and convection patterns in the two hemispheres. J Geophys Res Space Phys 120:9368–9384. https://doi.org/10.1002/2015JA021579. **arXiv:1606.01074**

Tenfjord P, Østgaard N, Haaland S, Snekvik K, Laundal KM, Reistad JP, Strangeway R, Milan SE, Hesse M, Ohma A (2018) How the IMF B_y Induces a Local B_y Component During Northward IMF B_z and Characteristic Timescales. J Geophys Res Space Phys 123:3333–3348. https://doi.org/10.1002/2018JA025186. **arXiv:1808.05034**.

Tsyganenko NA, Fairfield DH (2004) Global shape of the magnetotail current sheet as derived from Geotail and Polar data. J Geophys Res Space Phys 109:03218. https://doi.org/10.1029/2003JA010062

Tsyganenko NA, Andreeva VA, Gordeev EI (2015) Internally and externally induced deformations of the magnetospheric equatorial current as inferred from spacecraft data. Annales Geophysicae 33:1–11. https://doi.org/10.5194/angeo-19-1207-20017

Tsyganenko NA, Karlsson SBP, Kokubun S, Yamamoto T, Lazarus AJ, Ogilvie KW, Russell CT, Slavin JA (1998) Global configuration of the magnetotail current sheet as derived from Geotail, Wind, IMP 8 and ISEE 1/2 data. J Geophys Res 103:6827–6842. https://doi.org/10.1029/97JA03621

Xiao S, Zhang T, Ge Y, Wang G, Baumjohann W, Nakamura R (2016) A statistical study on the shape and position of the magnetotail neutral sheet. Annales Geophysicae 34:303–311. https://doi.org/10.5194/angeo-34-303-20169

Zhang TL, Baumjohann W, Nakamura R, Balogh A, Glassmeier K-H (2002) A wavy twisted neutral sheet observed by CLUSTER. Geophys Res Lett 29:1899. https://doi.org/10.1029/2002GL015544

Zhang TL, Nakamura R, Volwerk M, Runov A, Baumjohann W, Eichelberger HU, Carr C, Balogh A, Sergeev V, Shi JK, Fornacon K-H (2005) Double Star/Cluster observation of neutral sheet oscillations on 5 August 2004. Annales Geophysicae 23:2909–2914. https://doi.org/10.5194/angeo-23-2713-20051

Publisher's Note